Spontaneous *CP* violation electroweak baryogenesis and gravitational wave through multistep phase transitions

Songtao Liu and Lei Wang[*]

Department of Physics, Yantai University, Yantai 264005, People's Republic of China

In a singlet pseudoscalar extension of the two-Higgs-doublet model, we discuss spontaneous *CP* violation electroweak baryogenesis via two different patterns of phase transitions (PTs): (i) two-step PTs whose first step and second step are strongly first order; (ii) three-step PTs whose first step is second order and the second step and third step are strongly first order. For the case of the two-step pattern, the first-step PT takes place at a high temperature, converting the origin phase into an electroweak symmetry-broken phase and breaking the *CP* symmetry spontaneously. Thus, the baryon number is produced during the first-step PT. At the second-step PT, the phase is converted into the observed vacuum at zero temperature, and the *CP* symmetry is restored. In both phases, the sphaleron processes are sufficiently suppressed, which keep the baryon number unchanged. For the case of the three-step PTs, the pseudoscalar field first acquires a nonzero vacuum expectation value (VEV), and VEVs of other fields still remain zero during the first-step PT. The following PTs and electroweak baryogenesis are similar to the case of the two-step PTs. In addition, the gravitational wave spectra can have one or two peaks through the two-step and the three-step PTs, and we discuss the detectability at the future gravitational wave detectors.

I. INTRODUCTION

The baryon asymmetry of the Universe (BAU) is one of the long-standing questions of particle physics and cosmology. The observed BAU from big bang nucleosynthesis is given by [1]

$$Y_B \equiv \rho_B/s = (8.2 - 9.2) \times 10^{-11}, \qquad (1)$$

where ρ_B is the baryon number density and s is the entropy density. Generating such an asymmetry dynamically needs to satisfy the well-known Sakharov conditions: baryon number violation, sufficient C and CP violation, and departure from thermal equilibrium [2]. A theoretically attractive mechanism is provided by the electroweak baryogenesis (EWBG) [3,4], which can be tested at current or future colliders, because it generally involves new physics around TeV. In the EWBG scenario, the baryon number is violated by a sphaleron process at high temperatures, and the out-of-equilibrium environment is realized by a strong first-order electroweak phase transition (SFOEWPT). The

standard model (SM) contains the electroweak sphaleron process, but it fails to provide the out-of-equilibrium and sufficient CP violation. Therefore, a successful EWBG asks for an extension of the SM with additional sources of CP violation and extra particles coupling to the Higgs sector producing a SFOEWPT, which can be realized in some typical extensions of the SM, such as the singlet extension of the SM (see, e.g., [5–18]) and the two-Higgs-doublet model (2HDM) (see, e.g., [19–34]).

The explicit breaking of CP may appear in the scalar couplings or Yukawa couplings, which can be severely constrained by the nonobservation of electric dipole moment (EDM) experiments [35]. Several cancellation mechanisms are proposed to make the CP violation large enough to achieve the EWBG while satisfying the EDM data [33,34,36,37]. On the other hand, a finite temperature spontaneous CP violation mechanism can naturally avoid the constraints of the EDM data, where the CP symmetry is spontaneously broken at the high temperature and it is restored after the electroweak PT. The spontaneous CP violation EWBG can be realized in the singlet complex scalar extension of the SM [17,18] and the singlet pseudoscalar extension of 2HDM [38], in which the singlet field first acquires a nonzero vacuum expectation value (VEV) while the electroweak symmetry remains unbroken. Next, a SFOEWPT takes place through the vacuum decay between the singlet field direction and the doublet field direction in which the net BAU is produced via the conventional EWBG mechanism.

[*]Corresponding author.
leiwang@ytu.edu.cn

In Ref. [38], the authors proposed the singlet pseudo-scalar extension of 2HDM to achieve the EWBG in which the spontaneous breaking of *CP* is driven by the VEV of the pseudoscalar in the early Universe. In this paper, we continue the study of Ref. [38] and discuss the spontaneous *CP* violation EWBG via two-step PTs and three-step PTs as well as the corresponding the gravitational wave (GW) signal. For the two-step PTs, the first step and second step are both strongly first order. For the three-step PTs, the first step is second order, and the second step and third step are strongly first order. The GW spectra could have one or two peaks through the two-step and the three-step PTs [39–41], and we discuss the detectability at the future GW detectors, such as LISA [42], Taiji [43], TianQin [44], Big Bang Observer (BBO) [45], Decihertz Interferometer

GW Observatory (DECIGO) [45], and Ultimate-DECIGO (U-DECIGO) [46].

Our work is organized as follows. In Sec. II, we will give a brief introduction on the model. In Secs. III and IV, we discuss the possibility of explaining the BAU and detecting the GW signal at the future space-based detectors. Finally, we give our conclusion in Sec. V.

II. A SINGLET PSEUDOSCALAR EXTENSION OF 2HDM

A singlet pseudoscalar S is introduced to the 2HDM, and the Higgs potential includes two parts: V_{2HDM} and V_S. They are, respectively, the pure potential of 2HDM and the potential containing the pseudoscalar S. The V_{2HDM} with a softly broken discrete Z_2 symmetry is written as

$$V_{2HDM} = m_{11}^2(\Phi_1^\dagger\Phi_1) + m_{22}^2(\Phi_2^\dagger\Phi_2) - [m_{12}^2\Phi_1^\dagger\Phi_2 + \text{H.c.}] + \frac{\lambda_1}{2}(\Phi_1^\dagger\Phi_1)^2 + \frac{\lambda_2}{2}(\Phi_2^\dagger\Phi_2)^2$$
$$+ \lambda_3(\Phi_1^\dagger\Phi_1)(\Phi_2^\dagger\Phi_2) + \lambda_4(\Phi_1^\dagger\Phi_2)(\Phi_2^\dagger\Phi_1) + [\lambda_5(\Phi_1^\dagger\Phi_2)^2 + \text{H.c.}]. \tag{2}$$

The Φ_1 and Φ_2 are complex Higgs doublets with hypercharge $Y = 1$:

$$\Phi_1 = \begin{pmatrix} \phi_1^+ \\ \frac{1}{\sqrt{2}}(v_1 + \phi_1 + i\eta) \end{pmatrix}, \qquad \Phi_2 = \begin{pmatrix} \phi_2^+ \\ \frac{1}{\sqrt{2}}(v_2 + \phi_2 + ih_3) \end{pmatrix}, \tag{3}$$

where v_1 and v_2 are the electroweak VEVs with $v^2 = v_1^2 + v_2^2 = (246~\text{GeV})^2$ and the ratio of the two VEVs is defined as $\tan\beta = v_2/v_1$.

The V_S containing the singlet pseudoscalar S is given by

$$V_S = \frac{1}{2}m_0^2 S^2 + \frac{\kappa_S}{24}S^4 + [i\mu S\Phi_2^\dagger\Phi_1 + \text{H.c.}]$$
$$+ \frac{\kappa_1}{2}S^2\Phi_1^\dagger\Phi_1 + \frac{\kappa_2}{2}S^2\Phi_2^\dagger\Phi_2. \tag{4}$$

Here, we assume that all coupling coefficients and mass terms are real, and the pseudoscalar S does not develop a VEV at zero temperature. As a result, the Higgs potential sector is *CP* conserved at zero temperature.

The potential minimization conditions require

$$m_{11}^2 = m_{12}^2 t_\beta - \frac{1}{2}v^2(\lambda_1 c_\beta^2 + \lambda_{345}s_\beta^2),$$
$$m_{22}^2 = m_{12}^2/t_\beta - \frac{1}{2}v^2(\lambda_2 s_\beta^2 + \lambda_{345}c_\beta^2),$$
$$m_0^2 + \frac{\kappa_1}{2}v^2 c_\beta^2 + \frac{\kappa_2}{2}v^2 s_\beta^2 > 0, \tag{5}$$

with the shorthand notations $t_\beta \equiv \tan\beta$, $s_\beta \equiv \sin\beta$, $c_\beta \equiv \cos\beta$, and $\lambda_{345} = \lambda_3 + \lambda_4 + \lambda_5$.

After spontaneous electroweak symmetry breaking, we can obtain the mass matrices of the Higgs fields from the scalar potential in Eqs. (2) and (4):

$$(\phi_1 \quad \phi_2)\begin{pmatrix} m_{12}^2 t_\beta + \lambda_1 v^2 c_\beta^2 & -m_{12}^2 + \frac{\lambda_{345}}{2}v^2 s_{2\beta} \\ -m_{12}^2 + \frac{\lambda_{345}}{2}v^2 s_{2\beta} & m_{12}^2/t_\beta + \lambda_2 v^2 s_\beta^2 \end{pmatrix}\begin{pmatrix} \phi_1 \\ \phi_2 \end{pmatrix}, \tag{6}$$

$$(\eta \quad h_3 \quad S)\begin{pmatrix} \bar{m}_{12}^2 t_\beta & -\bar{m}_{12}^2 & -\mu v s_\beta \\ -\bar{m}_{12}^2 & \bar{m}_{12}^2/t_\beta & \mu v c_\beta \\ -\mu v s_\beta & \mu v c_\beta & m_0^2 + \frac{\kappa_1}{2}v^2 c_\beta^2 + \frac{\kappa_2}{2}v^2 s_\beta^2 \end{pmatrix}$$
$$\times \begin{pmatrix} \eta \\ h_3 \\ S \end{pmatrix}, \tag{7}$$

$$(\phi_1^+ \quad \phi_2^+)\left[m_{12}^2 - \frac{1}{4}(\lambda_4 + \lambda_5)v^2 s_{2\beta}\right]\begin{pmatrix} t_\beta & -1 \\ -1 & 1/t_\beta \end{pmatrix}\begin{pmatrix} \phi_1^- \\ \phi_2^- \end{pmatrix}, \tag{8}$$

with $\bar{m}_{12}^2 = m_{12}^2 - \frac{1}{2}\lambda_5 v^2 s_{2\beta}$ and $s_{2\beta} = \sin 2\beta$.

The mass eigenstates are obtained from the original fields by the rotation matrices:

$$\begin{pmatrix} H \\ h \end{pmatrix} = \begin{pmatrix} c_\alpha & s_\alpha \\ -s_\alpha & c_\alpha \end{pmatrix} \begin{pmatrix} \phi_1 \\ \phi_2 \end{pmatrix}, \tag{9}$$

$$\begin{pmatrix} G^0 \\ A \\ X \end{pmatrix} = \begin{pmatrix} 1 & 0 & 0 \\ 0 & c_\theta & -s_\theta \\ 0 & s_\theta & c_\theta \end{pmatrix} \begin{pmatrix} c_\beta & s_\beta & 0 \\ -s_\beta & c_\beta & 0 \\ 0 & 0 & 1 \end{pmatrix} \begin{pmatrix} \eta \\ h_3 \\ S \end{pmatrix}, \tag{10}$$

$$\begin{pmatrix} G^\pm \\ H^\pm \end{pmatrix} = \begin{pmatrix} c_\beta & s_\beta \\ -s_\beta & c_\beta \end{pmatrix} \begin{pmatrix} \phi_1^\pm \\ \phi_2^\pm \end{pmatrix}, \tag{11}$$

where $c_\alpha \equiv \cos\alpha$, $s_\alpha \equiv \sin\alpha$, $c_\theta \equiv \cos\theta$, and $s_\theta \equiv \sin\theta$. The G^0 and $G^\pm$ are Goldstone bosons which are absorbed

as longitudinal components of the Z and $W^\pm$ bosons. The remaining physical states are two neutral *CP*-even states h and H, two neutral pseudoscalars A and X, and a pair of charged scalars $H^\pm$, and their masses are obtained by using the rotation matrices in Eqs. (9)–(11) to diagonalize the mass matrices in Eqs. (6)–(8). These scalar masses can determine other relevant parameters:

$$\mu = \frac{m_X^2 - m_A^2}{v} s_\theta c_\theta,$$

$$m_0^2 = m_A^2 s_\theta^2 + m_X^2 c_\theta^2 - \frac{\kappa_1}{2} v^2 c_\beta^2 - \frac{\kappa_2}{2} v^2 s_\beta^2. \tag{12}$$

The couplings λ_i ($i = 1, 2, 3, 4, 5$) are determined by

$$v^2\lambda_1 = \frac{m_H^2 c_\alpha^2 + m_h^2 s_\alpha^2 - m_{12}^2 t_\beta}{c_\beta^2}, \qquad v^2\lambda_2 = \frac{m_H^2 s_\alpha^2 + m_h^2 c_\alpha^2 - m_{12}^2 t_\beta^{-1}}{s_\beta^2},$$

$$v^2\lambda_3 = \frac{(m_H^2 - m_h^2)s_\alpha c_\alpha + 2m_{H^\pm}^2 s_\beta c_\beta - m_{12}^2}{s_\beta c_\beta}, \qquad v^2\lambda_4 = \frac{(\hat{m}_A^2 - 2m_{H^\pm}^2)s_\beta c_\beta + m_{12}^2}{s_\beta c_\beta},$$

$$v^2\lambda_5 = \frac{-\hat{m}_A^2 s_\beta c_\beta + m_{12}^2}{s_\beta c_\beta}, \tag{13}$$

with $\hat{m}_A^2 = m_A^2 c_\theta^2 + m_X^2 s_\theta^2$.

The general Yukawa interactions are written as

$$-\mathcal{L} = Y_{u2}\bar{Q}_L\tilde{\Phi}_2 u_R + Y_{d2}\bar{Q}_L\Phi_2 d_R + Y_{\ell2}\bar{L}_L\Phi_2 e_R$$
$$+ Y_{u1}\bar{Q}_L\tilde{\Phi}_1 u_R + Y_{d1}\bar{Q}_L\Phi_1 d_R + Y_{\ell1}\bar{L}_L\Phi_1 e_R + \text{H.c.}, \tag{14}$$

where $Q_L^T = (u_L, d_L)$, $L_L^T = (\nu_L, l_L)$, $\tilde{\Phi}_{1,2} = i\tau_2\Phi_{1,2}^*$, and $Y_{u1,2}$, $Y_{d1,2}$, and $Y_{\ell1,2}$ are 3×3 matrices in family space. In order to avoid the tree-level flavor-changing neutral current, we take the Yukawa interactions to be aligned [47,48]:

$$(Y_{u1})_{ii} = \frac{\sqrt{2}m_{ui}}{v}(c_\beta - s_\beta\kappa_u), \qquad (Y_{u2})_{ii} = \frac{\sqrt{2}m_{ui}}{v}(s_\beta + c_\beta\kappa_u),$$

$$(Y_{\ell1})_{ii} = \frac{\sqrt{2}m_{\ell i}}{v}(c_\beta - s_\beta\kappa_\ell), \qquad (Y_{\ell2})_{ii} = \frac{\sqrt{2}m_{\ell i}}{v}(s_\beta + c_\beta\kappa_\ell),$$

$$(X_{d1})_{ii} = \frac{\sqrt{2}m_{di}}{v}(c_\beta - s_\beta\kappa_d), \qquad (X_{d2})_{ii} = \frac{\sqrt{2}m_{di}}{v}(s_\beta + c_\beta\kappa_d), \tag{15}$$

where all the off-diagonal elements are zero. $i = 1, 2, 3$ is the index of generation, and $X_{d1,2} = V_{\text{CKM}}^\dagger Y_{d1,2} V_{\text{CKM}}$. From Eqs. (10), (14), and (15), we can obtain the Yukawa couplings

$$-\mathcal{L}_Y = \frac{m_f}{v} y_h^f h\bar{f}f + \frac{m_f}{v} y_H^f H\bar{f}f - i\frac{m_u}{v}\kappa_u c_\theta A\bar{u}\gamma_5 u + i\frac{m_d}{v}\kappa_d c_\theta A\bar{d}\gamma_5 d + i\frac{m_\ell}{v}\kappa_\ell c_\theta A\bar{\ell}\gamma_5\ell$$

$$- i\frac{m_u}{v}\kappa_u s_\theta X\bar{u}\gamma_5 u + i\frac{m_d}{v}\kappa_d s_\theta X\bar{d}\gamma_5 d + i\frac{m_\ell}{v}\kappa_\ell s_\theta X\bar{\ell}\gamma_5\ell + H^+\bar{u}V_{\text{CKM}}\left(\frac{\sqrt{2}m_d}{v}\kappa_d P_R - \frac{\sqrt{2}m_u}{v}\kappa_u P_L\right)d + \text{H.c.}$$

$$+ \frac{\sqrt{2}m_\ell}{v}\kappa_\ell H^+\bar{\nu}P_R e + \text{H.c.}, \tag{16}$$

where $y_h^f = \sin(\beta - \alpha) + \cos(\beta - \alpha)\kappa_f$ and $y_H^f = \cos(\beta - \alpha) - \sin(\beta - \alpha)\kappa_f$ with $f = u, d, \ell$.

III. ELECTROWEAK PHASE TRANSITION AND BARYOGENESIS

A. Relevant theoretical and experimental constraints

Before discussing the electroweak PT and EWBG, we first introduce relevant theoretical and experimental constraints. We identify the lightest CP-even Higgs boson h as the observed 125 GeV state and take $\sin(\beta - \alpha) = 1$ in order to avoid the constraints of the 125 GeV Higgs signal data, for which the tree-level couplings of h to the SM particles are the same as the SM. The h is assumed to have no exotic decay mode. In addition, according to the Yukawa couplings of the extra Higgs fields (H, $H^{\pm}$, A, and X) as shown in Eq. (16), we assume κ_u, κ_d, and κ_{ℓ} to be small enough to suppress the cross sections of $gg \to A(X, H)$, $gg \to A(X, H)f\bar{f}$, $gg \to tbH^-$, and $gb \to tH^-$ at the LHC, so that benchmark points BP1 and BP2

can satisfy the exclusion limits of searches for additional Higgs bosons at the LHC. Also, very small κ_u, κ_d, and κ_{ℓ} can satisfy flavor bounds like $b \to s\gamma$. The other effects induced by the three parameters are ignored in the following discussions.

The scalar potential of the model includes the potential of 2HDM and the potential involved with the singlet field S, which are constrained by the vacuum stability, perturbativity, and tree-level unitarity. There are detailed discussions in Refs. [49,50], and we employ the formulas in Refs. [49,50] to implement the theoretical constraints. The model can give additional corrections to the oblique parameters (S, T, U) via the self-energy diagrams exchanging extra Higgs fields (H, $H^{\pm}$, A, and X). For $\sin(\beta - \alpha) = 1$, the expressions of S, T, and U in the this model are approximately given as [51,52]

$$S = \frac{1}{\pi m_Z^2}[c_\theta^2 F_S(m_Z^2, m_H^2, m_A^2) + s_\theta^2 F_S(m_Z^2, m_H^2, m_X^2) - F_S(m_Z^2, m_{H^\pm}^2, m_{H^\pm}^2)],$$

$$T = \frac{1}{16\pi m_W^2 s_W^2}[-c_\theta^2 F_T(m_H^2, m_A^2) - s_\theta^2 F_T(m_H^2, m_X^2) + F_T(m_{H^\pm}^2, m_H^2) + c_\theta^2 F_T(m_{H^\pm}^2, m_A^2) + s_\theta^2 F_T(m_{H^\pm}^2, m_X^2)],$$

$$U = \frac{1}{\pi m_W^2}[F_S(m_W^2, m_{H^\pm}^2, m_H^2) - 2F_S(m_W^2, m_{H^\pm}^2, m_{H^\pm}^2) + c_\theta^2 F_S(m_W^2, m_{H^\pm}^2, m_A^2) + s_\theta^2 F_S(m_W^2, m_{H^\pm}^2, m_X^2)]$$

$$- \frac{1}{\pi m_Z^2}[c_\theta^2 F_S(m_Z^2, m_H^2, m_A^2) + s_\theta^2 F_S(m_Z^2, m_H^2, m_X^2) - F_S(m_Z^2, m_{H^\pm}^2, m_{H^\pm}^2)], \tag{17}$$

where

$$F_T(a, b) = \frac{1}{2}(a + b) - \frac{ab}{a - b}\log\left(\frac{a}{b}\right),$$

$$F_S(a, b, c) = B_{22}(a, b, c) - B_{22}(0, b, c), \tag{18}$$

with

$$B_{22}(a, b, c) = \frac{1}{4}\left[b + c - \frac{1}{3}a\right] - \frac{1}{2}\int_0^1 dx X \log(X - i\epsilon),$$

$$X = bx + c(1 - x) - ax(1 - x). \tag{19}$$

Taking the recent fit results of Ref. [1], we use the following values of S, T, and U:

$$S = -0.01 \pm 0.10, \qquad T = 0.03 \pm 0.12,$$
$$U = 0.02 \pm 0.11, \tag{20}$$

with the correlation coefficients

$$\rho_{ST} = 0.92, \qquad \rho_{SU} = -0.80, \qquad \rho_{TU} = -0.93. \tag{21}$$

B. Electroweak phase transition and bubble profiles

To analyze the electroweak PT, one needs the effective potential of the model at the finite temperature. We parametrize the neutral components of the two Higgs doublets:

$$\frac{1}{\sqrt{2}}(h_1 + i\eta) = \frac{1}{\sqrt{2}}A_1 e^{i\varphi_1}, \quad \frac{1}{\sqrt{2}}(h_2 + ih_3) = \frac{1}{\sqrt{2}}A_2 e^{i\varphi_2}. \tag{22}$$

From Eqs. (2) and (4), one finds that the effective potential depends on only the relative phase $\varphi_2 - \varphi_1$. Thus, we choose to rotate φ_1 to 0 and take h_1, h_2, h_3, and S as the field configurations. The complete effective potential at finite temperature includes the tree-level potential, the Coleman-Weinberg term [53], the finite temperature corrections [54], and the resummed daisy corrections [55,56], which is gauge dependent [57,58]. Here, we take a gauge invariant approximation, which keeps only the thermal mass terms in the high-temperature expansion in addition to the tree-level potential. Then the effective potential is written as

$$V_{\text{eff}}(h_1, h_2, a_2, S_1, T) = \frac{1}{2}(m_{11}^2 + \Pi_{h_1})h_1^2 + \frac{1}{2}(m_{22}^2 + \Pi_{h_2})h_2^2 + \frac{1}{2}(m_{22}^2 + \Pi_{h_3})h_3^2 - m_{12}^2 h_1 h_2$$
$$+ \frac{\lambda_1}{8}h_1^4 + \frac{\lambda_2}{8}(h_2^4 + h_3^4) + \frac{\bar{\lambda}_{345}}{4}h_1^2 h_3^2 + \frac{\lambda_{345}}{4}h_1^2 h_2^2 + \frac{\lambda_2}{4}h_2^2 h_3^2$$
$$+ \frac{1}{2}(m_0^2 + \Pi_S)S^2 + \mu S h_1 h_3 + \frac{\kappa_1}{4}S^2 h_1^2 + \frac{\kappa_2}{4}S^2(h_2^2 + h_3^2) + \frac{\kappa_S}{24}S^4, \tag{23}$$

with

$$\Pi_{h_1} = \left[\frac{9g^2}{2} + \frac{3g'^2}{2} + 6\lambda_1 + 4\lambda_3 + 2\lambda_4 + \kappa_1 + 6y_t^2 c_\beta^2\right]\frac{T^2}{24},$$
$$\Pi_{h_2} = \left[\frac{9g^2}{2} + \frac{3g'^2}{2} + 6\lambda_2 + 4\lambda_3 + 2\lambda_4 + \kappa_2 + 6y_t^2 s_\beta^2\right]\frac{T^2}{24},$$
$$\Pi_{h_3} = \Pi_{h_2},$$
$$\Pi_S = [4\kappa_1 + 4\kappa_2 + \kappa_S]\frac{T^2}{24}, \tag{24}$$

where $\bar{\lambda}_{345} = \lambda_3 + \lambda_4 - \lambda_5$ and $y_t = \frac{\sqrt{2}m_t}{v}$.

In a first-order PT, bubbles nucleate and expand, converting the high-temperature phase into the low-temperature one. The probability of tunneling at the temperature T per unit time per unit volume is given by [59–61]

$$\Gamma \approx A(T)e^{-S_3/T}, \tag{25}$$

where $A(T) \sim T^4$ is a prefactor and S_3 is a three-dimensional Euclidian action.

The Euclidian action is calculated with $O(3)$ symmetric solutions for the configurations h_1, h_2, h_3, and S, which are determined by differential equations [62]

$$\frac{d^2\varphi_i}{dr^2} + \frac{2}{r}\frac{d\varphi_i}{dr} = \frac{\partial V_{\text{eff}}}{\partial\varphi_i} \quad (i = 1, 2, 3, 4), \tag{26}$$

with the boundary conditions $d\varphi_i/dr|_{r=0} = 0$ and $\varphi_i(r = \infty) = \varphi_{if}$ with φ_{if} being the VEV of the phase outside the bubble. Here, $\varphi_{i=1,2,3,4}$ denote h_1, h_2, h_3, and S, and r is the spatial radial coordinate. The solutions are used to determine the value of S_3:

$$S_3 = 4\pi \int_0^\infty dr r^2 \left[\sum_{i=1}^4 \frac{1}{2}\left(\frac{d\varphi_i}{dr}\right)^2 + V_{\text{eff}}\right]. \tag{27}$$

At the nucleation temperature T_n, the thermal tunneling probability for bubble nucleation per horizon volume and per horizon time is of the order of one, and the conventional condition is $\frac{S_3(T)}{T}\big|_{T=T_n} \approx 140$.

The dynamics of the electroweak PT are characterized by two key parameters β and α. β characterizes roughly the inverse time duration of the strong first-order PT:

$$\frac{\beta}{H_n} = T\frac{d(S_3(T)/T)}{dT}\bigg|_{T=T_n}, \tag{28}$$

where H_n is the Hubble parameter at the nucleation temperature T_n. α is defined as the vacuum energy released from the phase transition normalized by the total radiation energy density ρ_R at T_n:

$$\alpha = \frac{\Delta\rho}{\rho_R} = \frac{\Delta\rho}{\pi^2 g_* T_n^4/30}, \tag{29}$$

where g_* is the effective number of relativistic degrees of freedom.

During the first SFOEWPT, the doublet fields develop nonzero VEVs, namely, yielding a transition from $(0, 0, 0)$ to $(\langle h_1\rangle, \langle h_2\rangle, \langle h_3\rangle)$. The *CP* violation comes directly from the spatial evolution of $\langle h_3\rangle$, which renders the top quark mass a complex-valued function of the spatial coordinate across the bubble wall. The electroweak sphaleron processes [63–65] can bias the *CP* asymmetry produced around the bubble wall into the baryon asymmetry. The condition that guarantees the produced baryon asymmetry inside the bubbles of the broken phase is not washed out by the electroweak sphalerons leads to a bound on the PT strength [66]:

$$\frac{\xi_{n1}}{T_{n1}} > 1.0, \tag{30}$$

where $\xi_{n1} = \sqrt{\langle h_1\rangle^2 + \langle h_2\rangle^2 + \langle h_3\rangle^2}$ and T_{n1} is the nucleation temperature for the first SFOEWPT.

As the temperature drops down to the T_{n2}, the second SFOEWPT takes place, in which the phase is converted into the observed vacuum at zero temperature, and the *CP* symmetry is restored. During the second SFOEWPT, the sphaleron processes are sufficiently suppressed in both phases, which keeps the baryon number unchanged.

In our calculations, we require that the potential has a global minimum at the point of $(\langle h_1\rangle = v_1, \langle h_2\rangle = v_2, \langle h_3\rangle = 0, \langle S\rangle = 0)$ at zero temperature, which is numerically calculated. Considering the constraints from theory and the oblique parameters, we take benchmark point 1 (BP1) and benchmark point 2 (BP2) to provide detailed discussions on the physical processes for the two-step PTs and three-step PTs, respectively, which are shown in Table I. Because of the constraints of the oblique parameters, m_H and $m_{H^\pm}$ for BP1 and BP2 are favored to have a small mass

TABLE I. Input and output parameters for BP1 and BP2 with $m_h = 125$ GeV and $\sin(\beta - \alpha) = 1$. Here, ξ_{n2} and ξ'_{n2} denote $\sqrt{\langle h_1 \rangle^2 + \langle h_2 \rangle^2 + \langle h_3 \rangle^2}$ of phases at the interior and exterior of the bubble from the second SFOEWPT. The first SFOEWPT is from the first step of two-step PTs and the second step of three-step PTs, and the second SFOEWPT is from the second step of two-step PTs and the third step of three-step PTs.

	$\tan\beta$	m_{12}^2 (GeV)^2	m_H (GeV)	m_A (GeV)	$m_{H^\pm}$ (GeV)	m_X (GeV)	s_θ	κ_1	κ_2	κ_s
BP1	0.867	4628.4	463.3	124.6	478.2	539.2	-0.372	9.294	7.176	0.881
BP2	1.084	2864.9	481.6	161.5	494.4	412.6	-0.325	7.198	4.361	10.677

	The first SFOEWPT		The second SFOEWPT		
	T_{n1} (GeV)	ξ_{n1}/T_{n1}	T_{n2} (GeV)	ξ_{n2}/T_{n2}	ξ'_{n2}/T_{n2}
BP1	71.86	1.24	34.82	6.11	4.72
BP2	62.48	1.20	58.11	2.39	1.66

splitting. From Eqs. (17) and (18), one can find that the correction of the model to the T parameter tends to decrease with $|m_H - m_{H^\pm}|$ and disappears for $m_H = m_{H^\pm}$. The pseudoscalar with a mass of 124.6 GeV for BP1 is allowed by the signal data of the observed 125 GeV Higgs signal at the LHC, since its couplings to WW and ZZ are absent, and the couplings to fermions are taken to be negligibly small. The phase histories for BP1 and BP2 are, respectively, exhibited in Figs. 1 and 2 on field configurations versus temperature plane. The numerical package CosmoTransitions [67] is used to analyze the PTs. As the Universe cools, there appear three different phases, and they follow two-step PTs for BP1. At very high temperatures, because of the contributions of the thermal mass terms, the minimum of the potential is at the origin and the electroweak symmetry is restored, namely, $(\langle h_1 \rangle, \langle h_2 \rangle, \langle h_3 \rangle, \langle S \rangle) = (0, 0, 0, 0)$ GeV. When the temperature decreases to 71.86 GeV, the system tunnels to the second phase at $(67.2, 28.1, 51.6, 28.5)$ GeV via the first SFOEWPT. Because h_3 and S acquire nonzero VEVs, the CP symmetry is broken spontaneously. As the temperature decreases, the system evolves along the second phase until $T = 34.82$ GeV and $(\langle h_1 \rangle, \langle h_2 \rangle, \langle h_3 \rangle, \langle S \rangle) = (123.5, 67.2, 85.4, 35.1)$ GeV. Then it tunnels to the third

phase at $(161.1, 139.2, 0, 0)$ GeV, and the CP symmetry is restored via the second SFOEWPT. Next, the system evolves along the third phase and ultimately ends in the observed vacuum at $T = 0$ GeV.

Figure 2 shows that the Universe undergoes three-step PTs for BP2. At $T = 83$ GeV, the S field acquires a nonzero VEV, and the VEVs of h_1, h_2, and h_3 still remain zero via a second-order PT. When the temperature decreases to 62.48 GeV, the system tunnels to a new phase at $(48.3, 25.8, 51.5, 39.8)$ GeV via the first SFOEWPT. As the temperature decreases, the system evolves along the phase until $T = 58.11$ GeV and $(\langle h_1 \rangle, \langle h_2 \rangle, \langle h_3 \rangle, \langle S \rangle) = (63.4, 42.7, 59.2, 34.3)$ GeV. Then it tunnels to the final phase at $(93.4, 103.1, 0, 0)$ GeV via the second SFOEWPT and ultimately ends in the observed vacuum at $T = 0$ GeV.

The bubble wall VEV profiles are determined by the solutions of the bounce equations in Eq. (26), which are approximately obtained by FindBounce [68]. The baryon number is produced during the first SFOEWPT, and the relevant calculation depends on the bubble wall profiles. Therefore, in Fig. 3, we show the wall profiles of the first SFOEWPT for BP1 and BP2.
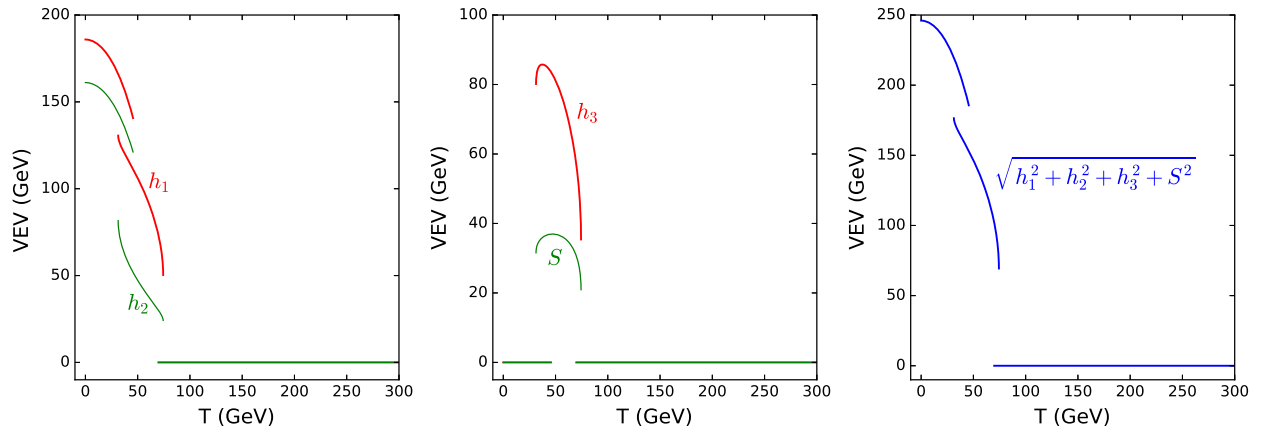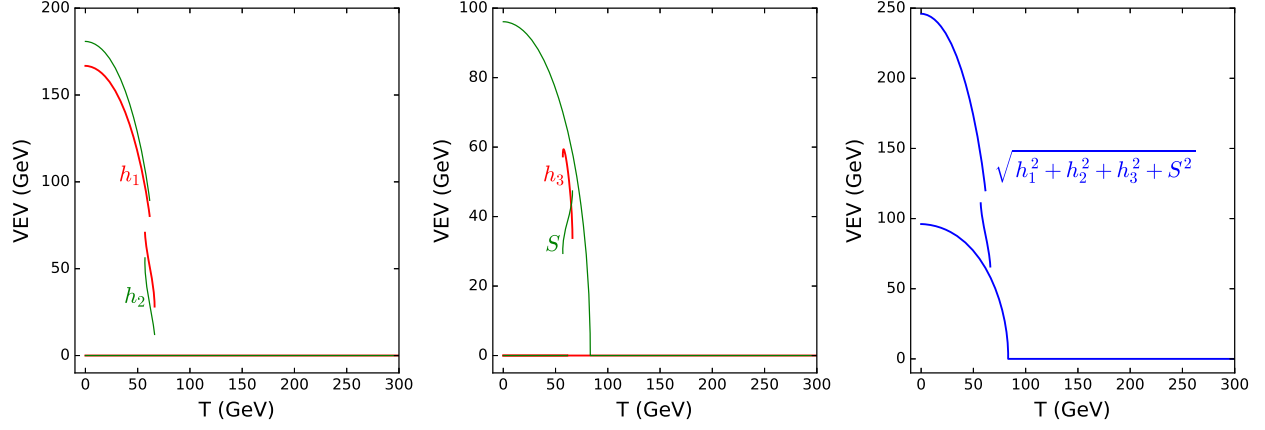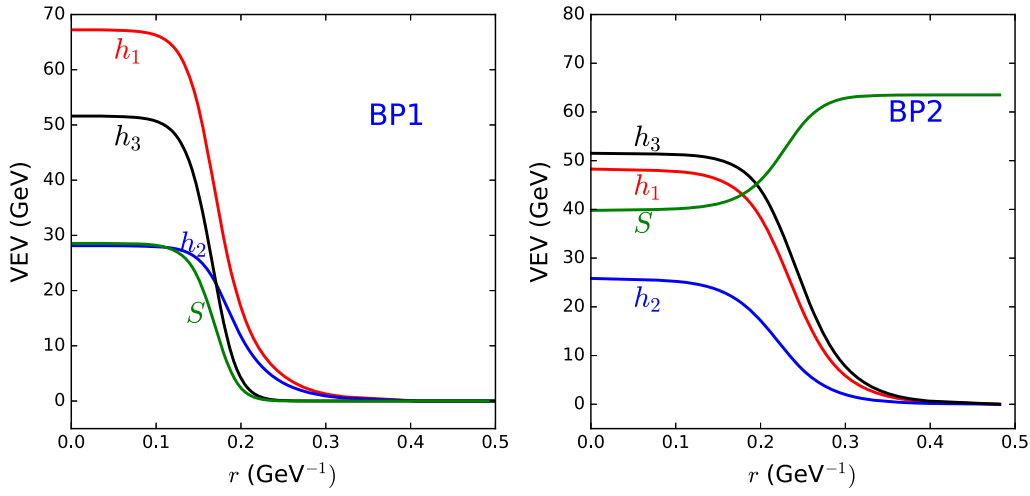

FIG. 1. Phase histories for BP1.

FIG. 2.   Phase histories for BP2.

FIG. 3.   The radial nucleation bubble wall VEV profiles of the first SFOEWPT for BP1 and BP2. Here, $r = 0$ is the center of the bubble.

C. Transport equations and baryon asymmetry

We take the WKB method to discuss the *CP*-violating source terms and chemical potential transport equations of particle species in the wall frame with a radial coordinate z [21,69,70]. The bubble wall is located at $z = 0$, with $z < 0$ and $z > 0$ pointing toward the interior and exterior of the bubble, respectively. In the model, the top quark plays the most important role in generating the BAU during the first SFOEWPT. It acquires a complex mass as a function of z when passing through the bubble wall whose profiles depend on the coordinate z. The mass of top quark is given as

$$m_t(z) = \frac{y_t}{\sqrt{2}} e^{i\varphi_Z(z)}(c_\beta h_1(z) + s_\beta\sqrt{h_2^2(z) + h_3^2(z)}e^{i\varphi_2(z)}),$$
$$= \frac{y_t}{\sqrt{2}}\sqrt{(c_\beta h_1(z) + s_\beta h_2(z))^2 + s_\beta^2 h_3^2(z)}\,e^{i\theta_t}, \quad (31)$$

with

$$\varphi_2(z) = \arctan\frac{h_3(z)}{h_2(z)},$$

$$\theta_t = \varphi_Z(z) + \arctan\frac{s_\beta h_3(z)}{c_\beta h_1(z) + s_\beta h_2(z)},$$

$$\partial_z\varphi_Z(z) = -\frac{h_2^2(z) + h_3^2(z)}{h_1^2(z) + h_2^2(z) + h_3^2(z)}\partial_z\varphi_2(z). \quad (32)$$

The addition phase $\varphi_Z(z)$ is from a local axial transformation of the top quark which removes the *CP*-violating force induced by the nonvanishing Z_μ field in the case of $\varphi_1 = 0$ [22].

The transport equations are derived for the top quark with a complex mass term and include effects of the strong sphaleron process (Γ_{ss}) [21,71], W scattering (Γ_W) [21,72], the top Yukawa interaction (Γ_y) [21,72], the top helicity flips (Γ_M) [21,72], and the Higgs number violation (Γ_h) [21,72]. The transport equations are given by
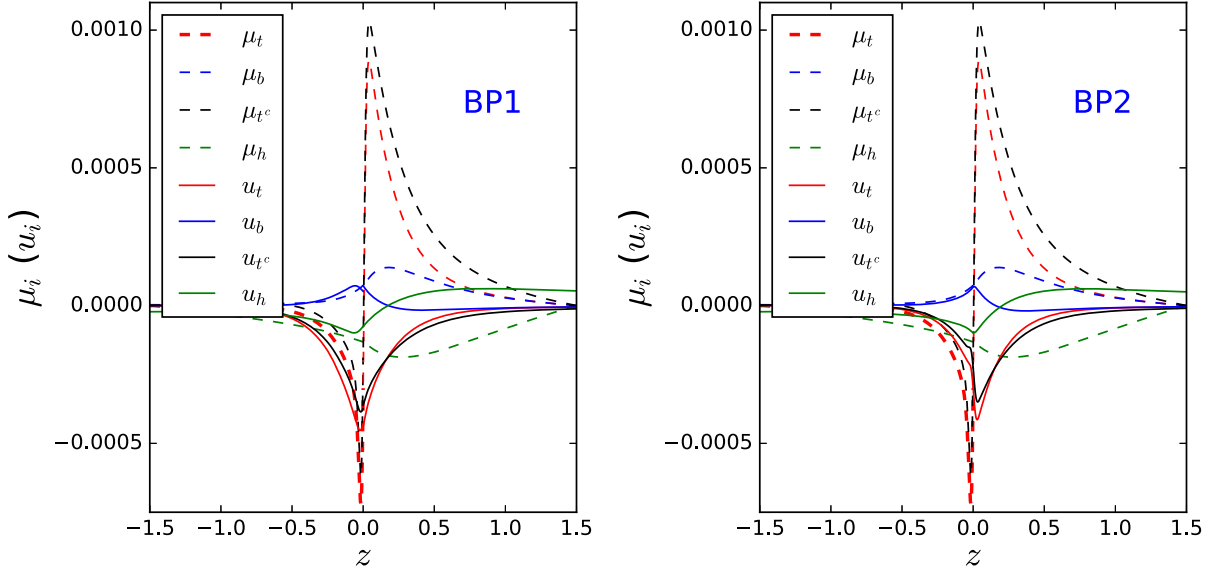
FIG. 4. For BP1 and BP2, the solutions to the transport equations for μ_i and u_i as functions of the coordinate z transverse to the bubble wall.

$$
\begin{aligned}
0 &= 3v_W K_{1,t}(\partial_z \mu_{t,2}) + 3v_W K_{2,t}(\partial_z m_t^2)\mu_{t,2} + 3(\partial_z u_{t,2}) \\
&\quad - 3\Gamma_y(\mu_{t,2} + \mu_{t^c,2} + \mu_{h,2}) - 6\Gamma_M(\mu_{t,2} + \mu_{t^c,2}) - 3\Gamma_W(\mu_{t,2} - \mu_{b,2}) \\
&\quad - 3\Gamma_{ss}[(1+9K_{1,t})\mu_{t,2} + (1+9K_{1,b})\mu_{b,2} + (1-9K_{1,t})\mu_{t^c,2}], \\
0 &= 3v_W K_{1,t}(\partial_z \mu_{t^c,2}) + 3v_W K_{2,t}(\partial_z m_t^2)\mu_{t^c,2} + 3(\partial_z u_{t^c,2}) \\
&\quad - 3\Gamma_y(\mu_{t,2} + \mu_{b,2} + 2\mu_{t^c,2} + 2\mu_{h,2}) - 6\Gamma_M(\mu_{t,2} + \mu_{t^c,2}) \\
&\quad - 3\Gamma_{ss}[(1+9K_{1,t})\mu_{t,2} + (1+9K_{1,b})\mu_{b,2} + (1-9K_{1,t})\mu_{t^c,2}], \\
0 &= 3v_W K_{1,b}(\partial_z \mu_{b,2}) + 3(\partial_z u_{b,2}) - 3\Gamma_y(\mu_{b,2} + \mu_{t^c,2} + \mu_{h,2}) - 3\Gamma_W(\mu_{b,2} - \mu_{t,2}) \\
&\quad - 3\Gamma_{ss}[(1+9K_{1,t})\mu_{t,2} + (1+9K_{1,b})\mu_{b,2} + (1-9K_{1,t})\mu_{t^c,2}], \\
0 &= 4v_W K_{1,h}(\partial_z \mu_{h,2}) + 4(\partial_z u_{h,2}) - 3\Gamma_y(\mu_{t,2} + \mu_{b,2} + 2\mu_{t^c,2} + 2\mu_{h,2}) - 4\Gamma_h \mu_{h,2}, \\
S_t &= -3K_{4,t}(\partial_z \mu_{t,2}) + 3v_W \tilde{K}_{5,t}(\partial_z u_{t,2}) + 3v_W \tilde{K}_{6,t}(\partial_z m_t^2)u_{t,2} + 3\Gamma_t^{\mathrm{tot}} u_{t,2}, \\
0 &= -3K_{4,b}(\partial_z \mu_{b,2}) + 3v_W \tilde{K}_{5,b}(\partial_z u_{b,2}) + 3\Gamma_b^{\mathrm{tot}} u_{b,2}, \\
S_t &= -3K_{4,t}(\partial_z \mu_{t^c,2}) + 3v_W \tilde{K}_{5,t}(\partial_z u_{t^c,2}) + 3v_W \tilde{K}_{6,t}(\partial_z m_t^2)u_{t^c,2} + 3\Gamma_t^{\mathrm{tot}} u_{t^c,2}, \\
0 &= -4K_{4,h}(\partial_z \mu_{h,2}) + 4v_W \tilde{K}_{5,h}(\partial_z u_{h,2}) + 4\Gamma_h^{\mathrm{tot}} u_{h,2}.
\end{aligned}
\tag{33}
$$

The $\mu_{i,2}$ and $u_{i,2}$ are the second-order CP-odd chemical potential and the plasma velocity of the particle $i = t, t^c, b, h$, respectively. The source term S_t is defined as

$$
S_t = -v_W K_{8,t}\partial_z(m_t^2 \partial_z \theta_t) + v_W K_{9,t}(\partial_z \theta_t)m_t^2(\partial_z m_t^2). \tag{34}
$$

The functions $K_{a,i}$ and $\tilde{K}_{a,i}$ ($a = 1-9$) are defined in Ref. [70], and the Γ_i^{tot} denotes the total reaction rate of the particle i [21,70]. We treat the wall velocity v_W as an input parameter and take $v_W = 0.1$.

The WKB method of calculating the source terms and transport equations is valid for $L_W T_n \gg 1$ with L_W being the width of bubble wall. We evaluate L_W by fitting the profile of the VEV with the hyperbolic tangent function:

$$
\sqrt{h_1^2(z) + h_2^2(z) + h_3^2(z)} = \frac{v_n}{2}\left(1 - \tanh\frac{z}{L_W}\right). \tag{35}
$$

Using this approach, one obtains $L_W T_{n1} \simeq 3.13$ and $L_W T_{n1} \simeq 3.68$ for the bubble wall of the first SFOEWPT of BP1 and BP2, respectively.

One solves the transport equations with the boundary conditions $\mu_i\ (z=\pm\infty)=0\ (i=t,t^c,b,h)$ and obtains the chemical potentials μ_i of each particle species. Using local baryon number conservation, the chemical potential of the left-handed quarks is then given by [69]

$$\mu_{B_L}=\frac{1}{2}(1+4K_{1,t})\mu_{t,2}+\frac{1}{2}(1+4K_{1,b})\mu_{b,2}-2K_{1,t}\mu_{t^c,2}.\tag{36}$$

Next, the weak sphalerons convert the left-handed quark number into a baryon asymmetry, which can be calculated with

$$Y_B=\frac{405\Gamma_{ws}}{4\pi^2 v_w g_* T_{n1}}\int_0^\infty dz\mu_{B_L}(z)\exp\left(-\frac{45\Gamma_{ws}}{4v_W}\right),\tag{37}$$

where $\Gamma_{ws}\simeq 1.0\times10^{-6}T_{n1}$ is the weak sphaleron rate inside the bubble [73]. Figure 4 shows the solutions to the transport equations for μ_i and u_i for BP1 and BP2, which give rise to the BAU, $Y_B\simeq 8.4\times10^{-11}$ for BP1 and $Y_B\simeq 8.3\times10^{-11}$ for BP2.

Notice that the effective potential $V_{\rm eff}$ has a Z_2 symmetry under which

$$h_3\to-h_3,\qquad S\to-S.\tag{38}$$

Therefore, there will not be a bias between transitions to $(\langle h_1\rangle,\langle h_2\rangle,\langle h_3\rangle,\langle S\rangle)$ and $(\langle h_1\rangle,\langle h_2\rangle,-\langle h_3\rangle,-\langle S\rangle)$ from the origin $(0,0,0,0)$ GeV. Thus, there are two kinds of bubbles relating to θ_t and $-\theta_t$, which produce baryon asymmetry of opposite signs. Eventually, the averaged baryon number is zero in the whole region due to their opposite signs. A soft Z_2 symmetry-breaking term $-\mu_3 S^3$ can be introduced to solve the problem. For BP2, the temperature of the Z_2-breaking PT is significantly higher than T_{n1} of the electroweak PT, and the regions with $-\langle S\rangle$ can vanish when the electroweak PT takes place. The needed condition is $\Delta V/T^4>10^{-16}$ with ΔV being the potential difference between the vacua with $\pm\langle S\rangle$ [74,75]. The μ_3 with a value of $\mathcal{O}(10^{-14})$ GeV can realize the condition for BP2. Unlike BP2, the vacua with $\pm\langle S\rangle$ for BP1 are still around at the time of the electroweak PT, but the volumes occupied by the $\pm\langle S\rangle$ phases can be significantly different. One can approximately estimate the ratio between the number densities of bubbles with a positive baryon number (N_+) and a negative baryon number (N_-) [76,77]:

$$\frac{N_+}{N_-}=\exp(-\Delta S_3/T),\tag{39}$$

with ΔS_3 being the S_3 difference between two types of bubbles. The global baryon density is given by

$$Y_B=Y_B^+\frac{N_+-N_-}{N_++N_-},\tag{40}$$

where Y_B^+ is the BAU generated from the bubble with $+\langle S\rangle$. For BP1, $Y_B\sim\frac{Y_B^+}{2}$ needs $\mu_3\sim\mathcal{O}(10^{-1})$ GeV, and such a value seems to be incompatible with the expected spontaneous *CP* violation, since the $\mu_3 S^3$ term breaks the *CP* symmetry explicitly.

IV. GRAVITATIONAL WAVE

There are three sources of GW production at a first-order PT: bubble collisions, sound waves in the plasma, and magnetohydrodynamic turbulence. We will focus on the GW spectrum from the sound waves in the plasma, which typically is the largest contribution among them. In addition to the two parameters β and α describing the dynamics of the PT, the GW spectra depends on the wall velocity with respect to the plasma at infinite distance, $\tilde{v}_W$. Note that $\tilde{v}_W$ can be significantly different from v_W [78], which is the relative wall velocity to plasma in front of the wall and relevant for baryogenesis. We take $\tilde{v}_W=0.6$ in our calculation.

The GW spectrum from the sound waves can be expressed by [79]

$$\Omega_{\rm sw}h^2=2.65\times10^{-6}\left(\frac{H_n}{\beta}\right)\left(\frac{\kappa_v\alpha}{1+\alpha}\right)^2\left(\frac{100}{g_*}\right)^{1/3}\tilde{v}_W$$
$$\times\left(\frac{f}{f_{\rm sw}}\right)^3\left(\frac{7}{4+3(f/f_{\rm sw})^2}\right)^{7/2}\Upsilon(\tau_{\rm sw}),\tag{41}$$

where $f_{\rm sw}$ is the present peak frequency of the spectrum:

$$f_{\rm sw}=1.9\times10^{-5}\frac{1}{\tilde{v}_W}\left(\frac{\beta}{H_n}\right)\left(\frac{T_n}{100\text{ GeV}}\right)\left(\frac{g_*}{100}\right)^{1/6}\text{ Hz}.\tag{42}$$

The κ_v is the fraction of latent heat transformed into the kinetic energy of the fluid [80]:

$$\kappa_v\simeq\kappa_B+(\tilde{v}_W-c_s)\delta\kappa+\frac{(\tilde{v}_W-c_s)^3}{(\xi_J-c_s)^3}[\kappa_C-\kappa_B-(\xi_J-c_s)\delta\kappa]$$
$$(\text{for }c_s<\tilde{v}_W<\xi_J),\tag{43}$$

with the sound velocity $c_s=\sqrt{1/3}$ and

$$\kappa_B\simeq\frac{\alpha^{2/5}}{0.017+(0.997+\alpha)^{2/5}},\qquad\kappa_C\simeq\frac{\sqrt{\alpha}}{0.135+\sqrt{0.98+\alpha}},$$

$$\xi_J\simeq\frac{\sqrt{\frac{2}{3}\alpha+\alpha^2}+\sqrt{1/3}}{1+\alpha},\qquad\delta\kappa\simeq-0.9\log\frac{\sqrt{\alpha}}{1+\sqrt{\alpha}}.\tag{44}$$
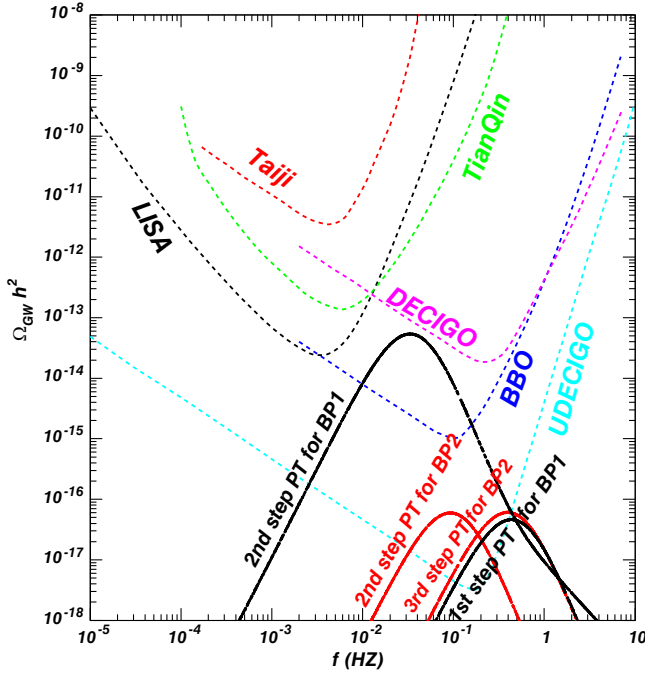
The suppression factor [81]

FIG. 5.   Gravitational wave spectra for BP1 and BP2.

$$\Upsilon(\tau_{sw}) = 1 - \frac{1}{\sqrt{1 + 2\tau_{sw}H_n}} \tag{45}$$

arises due to the finite lifetime τ_{sw} of the sound waves [82,83]:

$$\tau_{sw} = \frac{\tilde{v}_W(8\pi)^{1/3}}{\beta \bar{U}_f}, \qquad \bar{U}_f^2 = \frac{3}{4}\frac{\kappa_v \alpha}{1 + \alpha}. \tag{46}$$

We examine the GW spectra for BP1 and BP2, which are shown along with expected sensitivities of various future interferometer experiments in Fig. 5. For BP1, the GW spectra from the first-step and second-step PTs have peak frequencies around 0.44 and 0.03 Hz, respectively, and the peak strengths of the former and the latter exceed the sensitivity curves of U-DECIGO and BBO, respectively. For BP2, the GW spectra from the second-step and third-step PTs have peak frequencies around 0.09 and 0.39 Hz, respectively, whose peak strengths exceed the sensitivity curves of U-DECIGO. For BP2, the superposed GW spectra from the second step and third step have explicit double peaks, which can be observed by U-DECIGO. Note that there is still high uncertainty on the value of $\Upsilon(\tau_{sw})$,

and its determination needs considerable numerical simulations and analytical insights in the future. In addition, a full exploration of the parameter space will potentially find more promising regions for a detectable two-peaked GW signal at U-DECIGO.

V. CONCLUSION

In a singlet pseudoscalar extension of 2HDM, we studied the spontaneous *CP* violation EWBG via two-step PTs and three-step PTs and took BP1 and BP2 to perform detailed calculations. The first step of the two-step PTs is a SFOEWPT, which converts $(\langle h_1 \rangle, \langle h_2 \rangle, \langle h_3 \rangle, \langle S \rangle)$ into an electroweak symmetry-broken phase from $(0, 0, 0, 0)$ GeV and breaks the *CP* symmetry spontaneously. The electroweak sphaleron processes bias the *CP* asymmetry into the baryon number during the first-step PT. Also, the second step of the two-step PTs is a SFOEWPT, which converts the phase into the observed vacuum at zero temperature, and the *CP* symmetry is restored. However, the vacua with $\pm\langle S \rangle$ are still around at the time of the first SFOEWPT, and an explicit *CP*-violation term, $-\mu_3 S^3$ with $\mu_3 \sim (10^{-1})$ GeV, is required to guarantee the volumes occupied by the $\pm\langle S \rangle$ phases to be significantly different, leading to a sufficient baryon number density. The first step of the three-step PTs is a second-order PT during which the S field first develops a nonzero VEV, and VEVs of h_1, h_2, and h_3 still remain zero. Similar to the case of two-step PTs, the observed BAU is produced via the EWBG mechanism at the second step. The third step of the three-step PTs is a SFOEWPT, which converts the phase into the observed vacuum at the zero temperature and restores the *CP* symmetry. A very tiny *CP*-violation term, $-\mu_3 S^3$ with $\mu_3 \sim (10^{-14})$ GeV, is required to guarantee the regions with $-\langle S \rangle$ disappear when the second-step PT takes place. Meanwhile, the GW spectra through the two-step and three-step PTs can reach the sensitivities of BBO and U-DECIGO. Even more interesting is that a two-peaked GW signal could be observed at U-DECIGO.

[1] P. A. Zyla *et al.* (Particle Data Group), Review of particle physics, Prog. Theor. Exp. Phys. **2020,** 083C01 (2020).

[2] A. D. Sakharov, Violation of *CP* invariance, C asymmetry, and baryon asymmetry of the universe, Pisma Zh. Eksp. Teor. Fiz. **5,** 32 (1967).

[3] V. A. Kuzmin, V. A. Rubakov, and M. E. Shaposhnikov, On the anomalous Electroweak baryon number nonconservation in the early universe, Phys. Lett. **155B,** 36 (1985).

[4] V. A. Rubakov and M. E. Shaposhnikov, Electroweak nonconservation of the baryon number in the early universe and in high-energy particle collisions, Usp. Fiz. Nauk **166,** 493 (1996); Phys. Usp. **39,** 461 (1996).

[5] J. McDonald, Electroweak baryogenesis and dark matter via a gauge singlet scalar, Phys. Lett. B **323,** 339 (1994).

[6] J. McDonald, Cosmological domain wall evolution and spontaneous *CP*-violation from a gauge singlet scalar sector, Phys. Lett. B **357,** 19 (1995).

[7] G. C. Branco, D. Delepine, D. Emmanuel-Costa, and F. R. Gonzalez, Electroweak baryogenesis in the presence of an isosinglet quark, Phys. Lett. B **442,** 229 (1998).

[8] S. Profumo, M. J. Ramsey-Musolf, and G. Shaughnessy, Singlet Higgs phenomenology and the electroweak phase transition, J. High Energy Phys. 08 (2007) 010.

[9] V. Barger, P. Langacker, M. McCaskey, M. Ramsey-Musolf, and G. Shaughnessy, Complex singlet extension of the standard model, Phys. Rev. D **79,** 015018 (2009).

[10] M. Jiang, L. Bian, W. Huang, and J. Shu, Impact of a complex singlet: Electroweak baryogenesis and dark matter, Phys. Rev. D **93,** 065032 (2016).

[11] C.-W. Chiang, M. J. Ramsey-Musolf, and E. Senaha, Standard model with a complex scalar singlet: Cosmological implications and theoretical considerations, Phys. Rev. D **97,** 015005 (2018).

[12] F. P. Huang, Z. Qian, and M. Zhang, Exploring dynamical *CP* violation induced baryogenesis by gravitational waves and colliders, Phys. Rev. D **98,** 015014 (2018).

[13] K. P. Xie, Lepton-mediated electroweak baryogenesis, gravitational waves and the 4τ final state at the collider, J. High Energy Phys. 02 (2021) 090; 08 (2022) 52.

[14] J. Ellis, M. Lewicki, M. Merchand, J. M. No, and M. Zych, The scalar singlet extension of the Standard Model: Gravitational waves versus baryogenesis, J. High Energy Phys. 01 (2023) 093.

[15] M. Lewicki, M. Merchand, and M. Zych, Electroweak bubble wall expansion: Gravitational waves and baryogenesis in Standard Model-like thermal plasma, J. High Energy Phys. 02 (2022) 017.

[16] P. H. Ghorbani, Electroweak baryogenesis and dark matter via a pseudoscalar vs. scalar, J. High Energy Phys. 08 (2017) 058.

[17] W. Chao, *CP* violation at the finite temperature, Phys. Lett. B **796,** 102 (2019).

[18] B. Grzadkowski and D. Huang, Spontaneous *CP*-violating electroweak baryogenesis and dark matter from a complex singlet scalar, J. High Energy Phys. 08 (2018) 135.

[19] N. Turok and J. Zadrozny, Electroweak baryogenesis in the two doublet model, Nucl. Phys. **B358,** 471 (1991).

[20] J. M. Cline, K. Kainulainen, and A. P. Vischer, Dynamics of two Higgs doublet *CP* violation and baryogenesis at the electroweak phase transition, Phys. Rev. D **54,** 2451 (1996).

[21] L. Fromme, S. J. Huber, and M. Seniuch, Baryogenesis in the two-Higgs doublet model, J. High Energy Phys. 11 (2006) 038.

[22] J. M. Cline, K. Kainulainen, and M. Trott, Electroweak baryogenesis in two Higgs doublet models and B meson anomalies, J. High Energy Phys. 11 (2011) 089.

[23] S. Tulin and P. Winslow, Anomalous B meson mixing and baryogenesis, Phys. Rev. D **84,** 034013 (2011).

[24] T. Liu, M. J. Ramsey-Musolf, and J. Shu, Electroweak Beautygenesis: From $b \to s$ *CP*-Violation to the Cosmic Baryon Asymmetry, Phys. Rev. Lett. **108,** 221301 (2012).

[25] M. Ahmadvand, Baryogenesis within the two-Higgs-doublet model in the electroweak scale, Int. J. Mod. Phys. A **29,** 1450090 (2014).

[26] C. W. Chiang, K. Fuyuto, and E. Senaha, Electroweak baryogenesis with lepton flavor violation, Phys. Lett. B **762,** 315 (2016).

[27] H. K. Guo, Y. Y. Li, T. Liu, M. Ramsey-Musolf, and J. Shu, Lepton-flavored electroweak baryogenesis, Phys. Rev. D **96,** 115034 (2017).

[28] K. Fuyuto, W. S. Hou, and E. Senaha, Electroweak baryogenesis driven by extra top Yukawa couplings, Phys. Lett. B **776,** 402 (2018).

[29] T. Modak and E. Senaha, Electroweak baryogenesis via bottom transport, Phys. Rev. D **99,** 115022 (2019).

[30] P. Basler, M. Mühlleitner, and J. Müller, Electroweak baryogenesis in the *CP*-violating two-Higgs doublet model, Eur. Phys. J. C **83,** 57 (2023).

[31] P. Basler, M. Mühlleitner, and J. Müller, BSMPT v2 a tool for the electroweak phase transition and the baryon asymmetry of the universe in extended Higgs sectors, Comput. Phys. Commun. **269,** 108124 (2021).

[32] R. Zhou and L. Bian, Gravitational wave and electroweak baryogenesis with two Higgs doublet models, Phys. Lett. B **829,** 137105 (2022).

[33] K. Enomoto, S. Kanemura, and Y. Mura, Electroweak baryogenesis in aligned two Higgs doublet models, J. High Energy Phys. 01 (2022) 104.

[34] K. Enomoto, S. Kanemura, and Y. Mura, New benchmark scenarios of electroweak baryogenesis in aligned two Higgs double models, J. High Energy Phys. 09 (2022) 121.

[35] J. Baron *et al.* (ACME Collaboration), Order of magnitude smaller limit on the electric dipole moment of the electron, Science **343,** 269 (2014).

[36] L. Bian, T. Liu, and J. Shu, Cancellations between Two-Loop Contributions to the Electron Electric Dipole Moment with a *CP*-Violating Higgs Sector, Phys. Rev. Lett. **115,** 021801 (2015).

[37] S. Kanemura, M. Kubota, and K. Yagyu, Aligned *CP*-violating Higgs sector canceling the electric dipole moment, J. High Energy Phys. 08 (2020) 026.

[38] S. J. Huber, K. Mimasu, and J. M. No, Baryogenesis from spontaneous *CP* violation in the early Universe, Phys. Rev. D **107,** 075042 (2023).

[39] M. Aoki, T. Komatsu, and H. Shibuya, Possibility of a multistep electroweak phase transition in the two-Higgs doublet models, Prog. Theor. Exp. Phys. **2022,** 063B05 (2022).

[40] Q. H. Cao, K. Hashino, X. X. Li, and J. H. Yu, Multi-step phase transition and gravitational wave from general $\mathbb{Z}_2$ scalar extensions, arXiv:2212.07756.

[41] S. Fabian, F. Goertz, and Y. Jiang, Dark matter and nature of electroweak phase transition with an inert doublet, J. Cosmol. Astropart. Phys. 09 (2021) 011.

[42] H. Audley *et al.* (LISA Collaboration), Laser interferometer space antenna, arXiv:1702.00786.

[43] X. Gong *et al.*, Descope of the ALIA mission, J. Phys. Conf. Ser. **610**, 012011 (2015).

[44] J. Luo *et al.* (TianQin Collaboration), TianQin: A space-borne gravitational wave detector, Classical Quantum Gravity **33**, 035010 (2016).

[45] K. Yagi and N. Seto, Detector configuration of DECIGO/BBO and identification of cosmological neutron-star binaries, Phys. Rev. D **83**, 044011 (2011).

[46] H. Kudoh, A. Taruya, T. Hiramatsu, and Y. Himemoto, Detecting a gravitational-wave background with next-generation space interferometers, Phys. Rev. D **73**, 064006 (2006).

[47] A. Pich and P. Tuzon, Yukawa alignment in the two-Higgs-doublet model, Phys. Rev. D **80**, 091702 (2009).

[48] L. Wang and X. F. Han, Status of the aligned two-Higgs-doublet model confronted with the Higgs data, J. High Energy Phys. 04 (2014) 128.

[49] A. Drozd, B. Grzadkowski, J. F. Gunion, and Y. Jiang, Extending two-Higgs-doublet models by a singlet scalar field- the case for dark matter, J. High Energy Phys. 11 (2014) 105.

[50] X.-G. He and J. Tandean, New LUX and PandaX-II results illuminating the simplest Higgs-portal dark matter models, J. High Energy Phys. 12 (2016) 074.

[51] H.-J. He, N. Polonsky, and S. Su, Extra families, Higgs spectrum and oblique corrections, Phys. Rev. D **64**, 053004 (2001).

[52] H. E. Haber and D. ONeil, Basis-independent methods for the two-Higgs-doublet model. III. The *CP*-conserving limit, custodial symmetry, and the oblique parameters S, T, U, Phys. Rev. D **83**, 055017 (2011).

[53] S. R. Coleman and E. J. Weinberg, Radiative corrections as the origin of spontaneous symmetry breaking, Phys. Rev. D **7**, 1888 (1973).

[54] L. Dolan and R. Jackiw, Symmetry behavior at finite temperature, Phys. Rev. D **9**, 3320 (1974).

[55] P. B. Arnold and O. Espinosa, The effective potential and first order phase transitions: Beyond leading-order, Phys. Rev. D **47**, 3546 (1993); **50**, 6662(E) (1994).

[56] R. R. Parwani, Resummation in a hot scalar field theory, Phys. Rev. D **45**, 4695 (1992).

[57] R. Jackiw, Functional evaluation of the effective potential, Phys. Rev. D **9**, 1686 (1974).

[58] H. H. Patel and M. J. Ramsey-Musolf, Baryon washout, electroweak phase transition, and perturbation theory, J. High Energy Phys. 07 (2011) 029.

[59] I. Affleck, Quantum Statistical Metastability, Phys. Rev. Lett. **46**, 388 (1981).

[60] A. D. Linde, Decay of the false vacuum at finite temperature, Nucl. Phys. **B216**, 421 (1983); **B223**, 544(E) (1983).

[61] A. D. Linde, Fate of the false vacuum at finite temperature: Theory and applications, Phys. Lett. **100B**, 37 (1981).

[62] A. D. Linde, Fate of the false vacuum at finite temperature: Theory and applications, Phys. Lett. **100B**, 37 (1981).

[63] F. R. Klinkhamer and N. S. Manton, A saddle point solution in the Weinberg-Salam theory, Phys. Rev. D **30**, 2212 (1984).

[64] M. B. Gavela, P. Hernández, J. Orloff, O. Pene, and C. Quimbay, Standard Model *CP*-violation and baryon asymmetry. Part 2: Finite temperature, Nucl. Phys. **B430**, 382 (1994).

[65] P. Huet and E. Sather, Electroweak baryogenesis and Standard Model *CP*-violation, Phys. Rev. D **51**, 379 (1995).

[66] G. D. Moore, Measuring the broken phase sphaleron rate nonperturbatively, Phys. Rev. D **59**, 014503 (1999).

[67] C. L. Wainwright, CosmoTransitions: Computing cosmological phase transition temperatures and bubble profiles with multiple fields, Comput. Phys. Commun. **183**, 2006 (2012).

[68] V. Guada, M. Nemevšek, and M. Pintar, FindBounce: Package for multi-field bounce actions, Comput. Phys. Commun. **256**, 107480 (2020).

[69] J. M. Cline, M. Joyce, and K. Kainulainen, Supersymmetric electroweak baryogenesis, J. High Energy Phys. 07 (2000) 018.

[70] L. Fromme and S. J. Huber, Top transport in electroweak baryogenesis, J. High Energy Phys. 03 (2007) 049.

[71] G. F. Giudice and M. E. Shaposhnikov, Strong sphalerons and electroweak baryogenesis, Phys. Lett. B **326**, 118 (1994).

[72] P. Huet and A. E. Nelson, Electroweak baryogenesis in supersymmetric models, Phys. Rev. D **53**, 4578 (1996).

[73] G. D. Moore, Sphaleron rate in the symmetric electroweak phase, Phys. Rev. D **62**, 085011 (2000).

[74] J. R. Espinosa, B. Gripaios, T. Konstandin, and F. Riva, Electroweak baryogenesis in non-minimal composite Higgs models, J. Cosmol. Astropart. Phys. 01 (2012) 012.

[75] J. McDonald, Electroweak baryogenesis and dark matter via a gauge singlet scalar, Phys. Lett. B **323**, 339 (1994).

[76] D. Comelli, M. Pietroni, and A. Riotto, Spontaneous *CP* violation and baryogenesis in the minimal supersymmetric standard model, Nucl. Phys. **B412**, 441 (1994).

[77] G. W. Anderson and L. J. Hall, The Electroweak phase transition and baryogenesis, Phys. Rev. D **45**, 2685 (1992).

[78] J. M. No, Large gravitational wave background signals in electroweak baryogenesis scenarios, Phys. Rev. D **84**, 124025 (2011).

[79] M. Hindmarsh, S. J. Huber, K. Rummukainen, and D. J. Weir, Numerical simulations of acoustically generated gravitational waves at a first order phase transition, Phys. Rev. D **92**, 123009 (2015).

[80] J. R. Espinosa, T. Konstandin, J. M. No, and G. Servant, Energy budget of cosmological first-order phase transitions, J. Cosmol. Astropart. Phys. 06 (2010) 028.

[81] H.-K. Guo, K. Sinha, D. Vagie, and G. White, Phase transitions in an expanding universe: Stochastic gravitational waves in standard and non-standard histories, J. Cosmol. Astropart. Phys. 01 (2021) 001.

[82] J. Ellis, M. Lewicki, and J. M. No, Gravitational waves from first-order cosmological phase transitions: Lifetime of the sound wave source, J. Cosmol. Astropart. Phys. 07 (2020) 050.

[83] X. Wang, F. P. Huang, and X. Zhang, Phase transition dynamics and gravitational wave spectra of strong first-order phase transition in supercooled universe, J. Cosmol. Astropart. Phys. 05 (2020) 045.